I	Second moment of area (m^4)
l	Panel length (m)
$\hat{m}$	Mass index (kg/m^2)
P	Performance metric
$\hat{P}^+$	Maximum load index (N/m^2)
$\hat{Q}$	Heat transfer index (W/m^2K)
r	Volume ratio of face material in sandwich material
t	Face sheet thickness (m)
z	Smallest loading contact dimension (m)
Z	Penalty ()

[1] S. M. Lee, *Dictionary of Compos. Mater. Technol.* Technomic Publishing, Lancaster **1995**.

[2] DOGMA. *Design Optimisation and Guidelines for Multi-materials Appl.* **2000**, http://www.dogma.org.uk/.

[3] M. F. Ashby, Y. J. M. Bréchet, *Acta Mater.* **2003**, *51*, 5801.

[4] F. X. Kromm, J. M. Quenisset, R. Harry, T. Lorriot, *Mater. Design*, **2003**, *24*, 235.

[5] D. B. Miracle, S. L. Donaldson, in *ASM Handbook Volume 21: Compos.* ASM International **2001**.

[6] E. J. Barbero, *Int. to Compos. Mater. Design*, Taylor & Francis, London **1999**.

[7] M. F. Ashby, *Mater. Selection in Mech. Design*, Butterworth-Heinemann, Oxford **2005**.

[8] L. N. Phillips, *Design with Adv. Compos. Mater.* The Design Council, London **1989**.

[9] J. A. Quinn, *Compos. – Design Manual*, James Quinn Associates, Liverpool **1995**.

[10] CES, *Cambridge Eng. Selector* (software), Granta Design Ltd., Cambridge **2002**.

[11] S. M. Sapuan, H. S. Abdalla, *Compos. Part A*, **1998**, *29A*, 731.

[12] M. F. Ashby, *Acta Metall. Mater.* **1993**, *41*, 1313.

[13] P. Sirisalee, M. F. Ashby,G. T. Parks, P. J. Clarkson, *Adv. Eng. Mater.* **2004**, *6*, 84.

[14] P. Sirisalee, G. T. Parks, M. F. Ashby, P. J. Clarkson, in *Proc. of the ASME Design Eng. Technical Conf. (DETC/CIE 2004)*, Salt Lake City, Utah **2004**.

[15] J. Rasmussen, P. Staelens, in *Proc. of the Fourth Int. Conf. on Sandwich Constructions*, Stockholm, Sweden **1998**.

DOI: 10.1002/adem.200500185

Increasing the Strength/Toughness Combination of High Volume Fraction Particulate Metal Matrix Composites using an Al-Ag Matrix Alloy

By *Ali Miserez*, *Randoald Müller*, and *Andreas Mortensen**

Particulate reinforced metal matrix composites (PRMMCs) containing a high volume fraction of ceramic particles (> 50 vol.%) display an elastic stiffness that far exceeds that of aluminium and its alloys, at only a small cost in terms of density. If their microstructure is adequately designed and optimized, these materials can be made to exhibit strength/toughness combinations that match those of unreinforced high-strength engineering aluminium alloys.[1,2] The potential of these composites in energy-intensive structural applications is thus clearly high.

The elevated toughness of these composites is achieved by meeting certain critical microstructural conditions, defined and explained in.[1–4] To summarize, these include: (i) the initial (high) quality of the stiff ceramic particles used, which must be free of stress concentration sites and internal defects, (ii) the presence of a ductile matrix free of brittle second phases, (iii) a capacity for composite bulk plastic deformation, made possible in spite of the high ceramic loadings by the fact that only the metal is continuous in their microstructure. These characteristics combined produce, in the composite, a

[*] *R. Müller, Prof. A. Mortensen*
Laboratory for Mechanical Metallurgy
Institute of Materials
Swiss Federal Institute of Technology in Lausanne (EPFL)
MXD,Station 12
1015 Lausanne, Switzerland.
E-mail: andreas.mortensen@epfl.ch

Dr. A. Miserez
Now with: Materials Department
College of Engineering
University of California
Santa Barbara, CA 93'106-5050, USA.

[**] *This work was funded by the Swiss National Science Foundation under contract-no. 200020-107556, with added support from core funding of the Swiss Federal Institute of Technology, Lausanne. The authors gratefully acknowledge Metalor Technology S.A. for kindly donating the pure Ag flakes used in this work.*

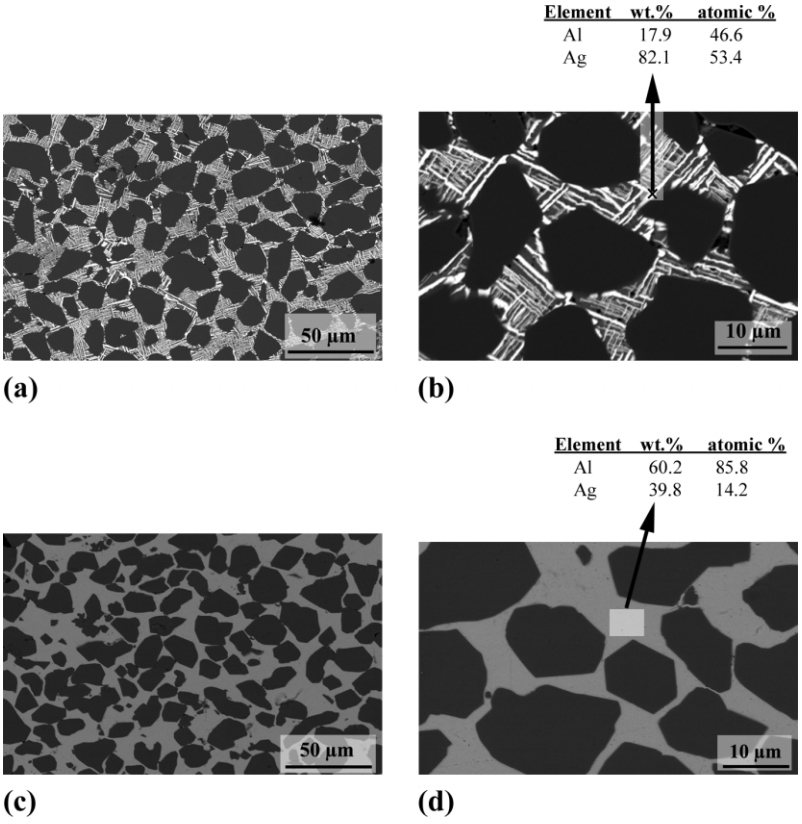

Fig. 1. SEM images in the backscattered mode of polished section of the composites. (a) and (b): as-cast condition; (c) and (d): after solution heat-treatment and subsequent peak-aging. In the as-cast condition, $AlAg_2$ precipitates (γ phase) in the shape of elongated plates (in bright) are formed between adjacent particles; after heat-treatment all coarse γ phases are dissolved.

local fracture cohesive law,[5,6] that features both (i) an elevated peak stress and (ii) a high local fracture energy. The ability for macroscopic plastic deformation in the composite then amplifies this local fracture energy, resulting in a high global composite fracture energy characteristic of the formation and propagation of a macroscopic plastic zone surrounding the tip of a propagating crack.

It was shown by alloying the aluminium matrix of these composites with copper that, when the above conditions are met, the fracture toughness and the tensile strength of these composites can be increased simultaneously by increasing the matrix flow stress σ_y, all else being constant.[1] We demonstrate here further simultaneous improvements in composite tensile strength and toughness, using a somewhat exotic matrix alloy, namely an alloy of aluminium with silver; we justify this choice in the next section.

Matrix Selection: There are, as mentioned above, several factors that practically limit the choice of the matrix alloy in high-performance metal matrix composites. The greatest concern is to avoid coarse brittle phases, such as intermetallics or silicon. Such embrittling phases can form at various stages of composite processing: by reaction between the matrix and the reinforcement, during solidification, or during heat-treatment.[7–14] Even small quantities of brittle second phases, particularly if these are located along the matrix/reinforcement interface, are well-documented to affect the toughness and tensile ductility of metal matrix composites,[13–19] particularly when they exceed a relatively small critical thickness.[20–24] A second factor in matrix selection is the need for strong interfacial bonding, this being especially important in particulate composites.

These considerations previously led us to select pure Al and Al-Cu binary alloys containing less than the maximum solid solubility limit of 5.65 wt.% Cu as the matrix of alumina particle reinforced composites.[1] Al_2O_3 being furthermore chemically inert with both Al and Cu at all processing temperatures, these matrices could be produced free of intermetallics or interfacial reaction products (with the exception of a few residual Al-Cu-Fe phases caused by iron impurities in the matrix). Aluminium alloys with a higher strength than Al-Cu alloys are generally alloyed with magnesium (most 2xx or 2xxx series alloys and all 7xxx series alloys contain Mg). Magnesium in aluminium unfortunately reacts with alumina, causing the formation of brittle interfacial reaction products.[7,9] We therefore explore here another, more unusual, alloying addition that is documented to yield high strength in aluminium while not being prone to react with alumina, namely silver.

Silver is highly soluble in aluminium: the peak solubility of Ag in Al is about 55 wt.% (23.5 at.%) at 567 °C.[25,26] With such a high amount of solute in the matrix, it is expected that a matrix flow stress exceeding that of peak-aged Al-4.5 wt.% Cu can be produced in this system. Al-40 wt.% Ag (corresponding to 15 at.% Ag) was therefore selected. This alloy can be solutionized in the α single-phase field. It age-hardens by GP zone formation; these are followed by γ (Ag_2Al) precipitates growing in the form of fine Widmanstätten plates.[25–28] There also exists in the Al-Ag phase diagram a spinodal region with a critical composition that is near the selected alloy composition (at approximately 20 at.%).[29] Hence, this matrix can also be quenched to a tem-

Table 1. Mechanical properties (tensile, hardness) of Al-40 wt.%Ag matrix composites in the various heat-treatment conditions. For comparison with other composites and Al alloys, the density of the composites is also indicated in the table.

Heat-treatment	E [GPa]	$\sigma_{0.2}$ [MPa]	U.T.S. [MPa]	ε_f [%]	Vickers Hardness	ρ [g/cm3]
As-cast (AC)	176	350	396	0.77	197	3.84
Solution treated (ST)	181	436	461	0.60	265	"
Peak aged (T6)	179	503	509	0.48	319	"

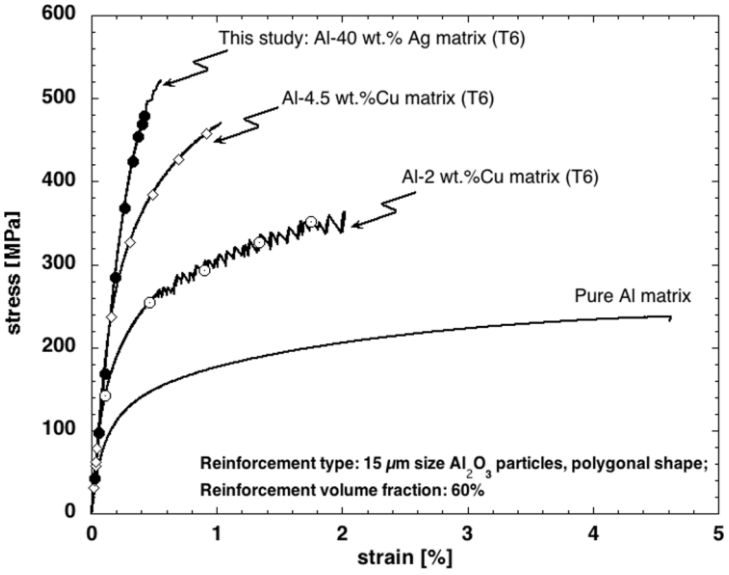

Fig. 2. Tensile curves of the composite (peak-aged condition) and comparison with previous data on analogous composites with the same reinforcement varying the matrix. Data for pure Al matrix composite are from, [52] for Al-Cu matrix composites from. [1]

perature where spinodal decomposition, and nucleation and growth, of γ plates occur simultaneously.[29] The main drawback of this model system is that, although Al-Ag alloys have been explored to study precipitation hardening and spinodal decomposition, precise data on their mechanical behaviour, including basic mechanical properties such as flow stress, are scarce in the literature. Another drawback is of course the fact that such alloys are less attractive than Al-Cu alloys from an engineering standpoint: Al-40 wt.% Ag is clearly more dense and much more expensive than Al-4.5 wt.% Cu.

With no interfacial reactivity, no brittle intermetallics, and a higher flow stress than peak-aged Al- Al-4.5 wt.% Cu, if our interpretation of the properties of these composites is correct a matrix of Al-40 wt.% Ag should simultaneously increase the tensile strength and the fracture toughness of these composites. We show in what follows that this is, indeed, observed.

Results. Microstructure: Electron micrographs of the composites are shown in Figure 1. In the as-cast condition (Fig. 1(a) and 1(b)), the matrix is multiphase: in the BSE detector mode, Ag-containing second phases appear bright and in clear contrast from the a solid solution. The higher magnification micrograph in Figure 1(b) shows that the Ag-rich phases have an elongated plate-like structure contacting adjacent particles. According to the Al-Ag phase diagram, these plates are of the Ag_2Al (γ phase) intermetallic compound. Semi-quantitative compositions obtained by EDX on individual spots of the bright phases are given in the inset of Figure 1(b). These confirm a high silver concentration within the plate, although the measured at.% value remains below that of the γ phase (a more precise quantification than possible by EDX in the single-spot mode was not deemed necessary).

After solid-solution treatment, quenching and aging, the large γ plates are dissolved, Figures 1(c,d). In particular, the higher magnification micrograph in Figure 1(d) indicates that no coarse residual intermetallic phases remains after heat-treatment. This is in contrast with corresponding Al-Cu matrix composites, where Fe impurities prevented complete solution of a small fraction of the intermetallics.[10] Elemental compositions measured by EDX in the window inset of Figure 1(c) indicate an Al:Ag weight ratio of 60:40; this is fully coherent with the nominal composition of the matrix alloy.

Mechanical Properties. Tensile testing: Average values of tensile properties of the composites in the various heat-treatment conditions are given in Table 1. A typical tensile curve of the present composite after solid solution treatment and subsequent peak aging is presented in Figure 2, together with other curves from our previous study of similar Al-Cu and pure Al matrix composites. A slight increase in the flow stress and UTS is noticed for the current Al-Ag matrix composites. At the same time, the strain to failure decreases to about 0.5 % and there is little macroscopic plastic deformation prior to failure, such that $\sigma_{0.2}$ and UTS are nearly equivalent, falling in the range 500 – 520 MPa. The Young's modulus remains on the order of 180 GPa.

Fracture toughness and validity criteria: Fracture toughness values inferred form chevron-notch fracture testing are given in Table 2. A typical chevron-notch curve for a peak-aged Al-Ag matrix composite is presented in Figure 4, together with a similar curve from an Al-4.5 wt. % Cu T6 matrix composite. A few comments on the validity of the tests are necessary before presenting the data.

(1) The specimen size criterion necessary to ensure plane-strain conditions, and given by $B > 1.25\ (K_{Iv}/\sigma_y)^2$ for chevron-notched specimens, was met for all specimens at all heat-treatment conditions.

(2) There is an additional plasticity criterion in chevron-notch testing for the data to be validated; the definition of this criterion and its significance can be found in.[30–32] In the pres-

Table 2. Fracture toughness of Al-40 %Ag matrix composites as measured by chevron-notched testing. The crack length increment Δa_m at which crack deviation occurred (see text and Fig. 3) from stereomicroscope images are also indicated. The critical crack length at which the toughness is computed is $\Delta a_c = 5.45$ mm.

Heat-treatment	K_{Iv} [MPa$\sqrt{m}$]	Δa_m [mm]
AC	15.9	No crack deviation
ST	36.1	7.9
ST	36.4	8.3
T6	34.7	–
T6	37.6	7.1
T6	37.1	5.9

ent case, the value of the relevant parameter (the "*p*-value") was found to be negative; this is most likely due to residual stresses arising from the heat-treatment. Although negative *p*-values invalidate the data according to the Standard, we do not view this as a significant problem, mainly because *p*-values are strongly dependent on the precise method used in computing their value (see for instance the fracture curves presented in Fig. 4); the matter is further discussed by Grant *et al.*[32]

(3) In the present tests, the main issue potentially limiting validity of the data was a deviation of the crack from its nominal plane of propagation (along the chevron notch) for all heat-treated specimens. This may affect the validity of the data. More specifically, in chevron-notch testing, for a fixed load there exists a minimum in the curve giving the stress intensity *vs*. the crack length *a* (the crack driving force curve). The critical value at which this minimum is reached, a_c, is a function of the sample geometry. For an ideal elastic material exhibiting a flat *R*-curve, the crack length at the maximum load P_m is by definition a_c. At this point, both the stress-intensity factor and the crack length a_c are known, hence allowing to infer the toughness.[33] For materials showing limited *R*-curve behaviour, a compliance method is defined in the Standard, and here again the toughness is measured at this known critical crack length a_c. In the chevron-notch short-bar geometry used here, a_c equals 14.25 mm (corresponding to an adimensional value a_c/W of 0.537 where *W* is the specimen length), and the initial crack length a_0 equals 8.8 mm. The critical length a_c is thus attained after a crack increment Δa_c of 5.45 mm. The crack increment at which the crack deviated away from the chevron notch, Δa_m, was measured using stereomicroscope macrofractographs as indicated in Figure 3, for all samples that presented crack deviation (this point is clearly apparent from a top-view of the sample, Figure 3(b), as that where crack edges deviate from the machined chevron triangle). The values are given in Table 2. As seen, for all samples of this work, the crack left the chevron notch *after* reaching the stress intensity factor minimum; *i.e.*, $\Delta a_m > \Delta a_c$ (= 5.45 mm); Figure 3 illustrates this. Therefore, at the critical load used to infer the plane-strain fracture toughness of these samples, the crack was still in its main propagation plane. The present data are thus not invalidated by this effect (the influence of the finite crack plane curvature visible in Figure 3 at $a = a_c$ is small and ignored in what follows).

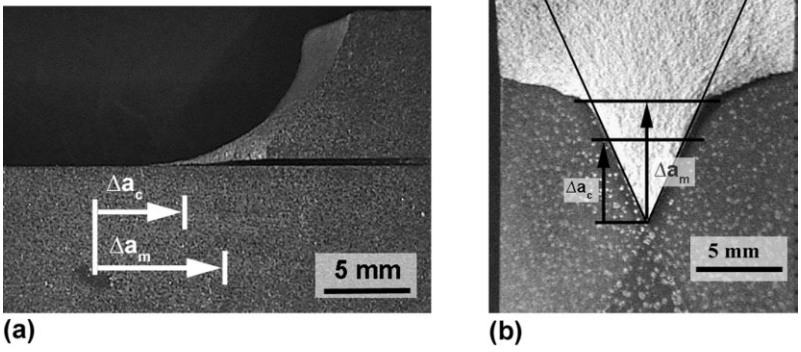

Fig. 3. Fracture surfaces of a chevron-notched specimen (T6 condition) taken by stereomicroscopy. (a) side-view illustrating deviation of the crack plane; (b) the top-view is used to measure at what length the crack deviated (this is seen by the abrupt enlargement of the crack front beyond the limits of the chevron triangle). In all specimens deviation occurred at a crack length a_m longer than the crack length a_c used to infer the fracture toughness in the chevron-notched geometry and fracture data can be validated. Corresponding distances Δa_c and Δa_m are reported from (b) on (a).

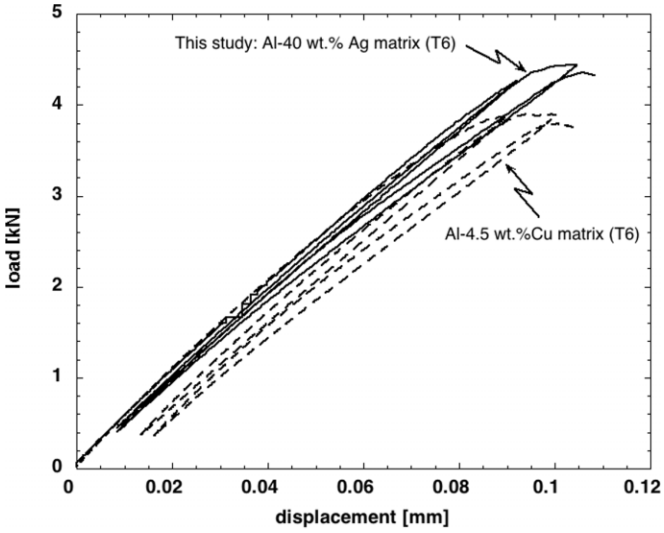

Fig. 4. Chevron-notched fracture curves of the present composites and comparison with previous data for analogous Al-4.5 wt.% Cu T6 matrix composites. The plane-strain chevron-notched fracture toughness, K_{Iv}, is measured from a load essentially equivalent to the peak load. Since the geometry of the two specimens is the same, the toughness scales essentially with the peak load.

As seen in Figure 4, despite a significant reduction in the tensile strain to failure (Fig. 2), the resistance to crack-propagation is higher than with the Al-Cu matrix. The recorded average K_{Iv} value is 36.5 $MPa\cdot m^{1/2}$ in the peak-aged condition for the present composites (with a maximum of 37.6 for one test), and 36.2 for the ST condition. By comparison, the composite in the as-cast condition is much more brittle, attaining only 15.9 $MPa\cdot m^{1/2}$, *i.e.*, less than half the value after heat-treatment.

Fracture Micromechanisms: SEM fractographs in the back-scattered electron imaging mode of chevron-notch specimens are presented in Figure 5. In the as-cast condition, the secondary phases previously observed on polished sections (Figs. 1(a,b)) are also clearly detected on the fracture surface in the form of the numerous bright elongated particles. As in Al-Cu matrix composites in the as-cast condition, premature cracking of these coarse intermetallic particles provides matrix cavitation nucleation sites; these also likely promote early ceramic particle cracking.

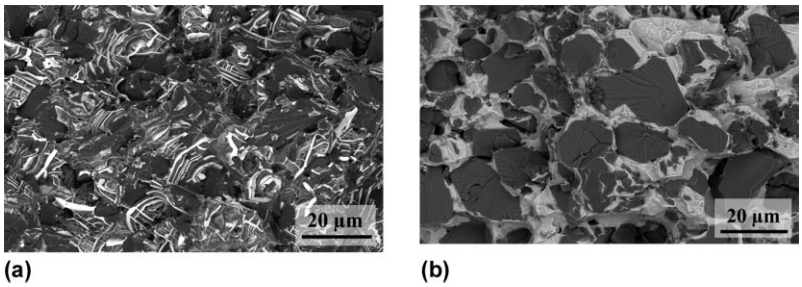

Fig. 5. SEM fractographs of the composites in the backscattered electron detector mode. (a) Composite in the as-cast conditions, showing coarse secondary phases; (b) heat-treated composite; note that all particles are broken on the fracture surface, as found in Ref. [1] for analogous composites with a peak-hardened Al-4.5 wt.% Cu matrix.

After solution heat-treatment and aging, coarse secondary phases are clearly absent from the fracture surface, Figure 5(b), consistent with Figure 1. Broken alumina particles, on the other hand, cover a large fraction of the fracture surface, more so than with an as-cast matrix. As shown in,[1] in such composites containing about 60 vol. %. ceramic particles, a fracture surface area that is covered by about 75 % broken particles means that essentially all particles along the crack path are cleaved during crack propagation: this is what we observe here. Between the particles, the matrix has fractured in a ductile fashion, leaving plastic tearing ridges commensurate with the space between particles, Figure 5(b). Overall, the fracture surface of aged Al-Ag composites thus resembles that of similar composites with a matrix of Al-4.5 wt.% Cu in the T4 or T6 condition.

Discussion: With an Al-4.5 wt.% Cu matrix in similar composites, optimal property combinations were obtained after heat-treatment with the same 15 µm polygonal alumina particles as those used here. The ultimate tensile strength reached 480 MPa and the fracture toughness, also measured using the chevron-notch technique, was 34 $MPa\cdot m^{1/2}$. Comparatively, with the Al-Ag matrix the tensile strength is near 500 MPa, while the plane-strain fracture toughness is between 35 and 40 $MPa\cdot m^{1/2}$. Although not directly measured, the flow stress of the peak-aged Al-40 %Ag matrix is also higher than that of Al-4.5 %Cu matrix, as shown by the Vickers hardness (HV) data. The present data thus confirm that tensile strength and fracture toughness increase simultaneously when the matrix flow stress is raised, provided conditions listed in Section 2 are respected.

As with Al-4.5 wt.% Cu T6 matrix composites produced using the same polygonal alumina particles (these were from the same shipment), all particles are broken along the crack path in the present composites: this is expected from a stronger matrix. Referring to the toughening mechanisms proposed earlier for these composites,[1,2] if particle fracture remains the main crack advance mechanism, the local peak stress of the cohesive law must be roughly the same in both composites. The "amplification" factor by which the local (cohesive) fracture energy is increased cannot then be higher in the present composites than with Al-4.5 %Cu composites, since this factor is mainly governed by the ratio of peak cohesive stress to composite yield stress. Therefore, the increase in fracture toughness exhibited by the present composites must result from an increase in the local work of fracture. Indeed, since the micromechanisms of fracture for the two composites are essentially equivalent (formation of large matrix ligaments between broken particles under high stress triaxiality), the local work of fracture associated with the creation of the fracture surface should increase if the matrix flow stress increases, as expected from micromechanical models for the creation of ductile fracture profiles.[34–37]

The present data are combined with results from earlier studies in Figure 6, which also includes corresponding values for engineering aluminium alloys (empty boxes, from Ref.[38]), as well as data for other particle-reinforced MMCs from the literature (shaded boxes). To keep the plot readable, we have deliberately limited our choice of data in this last category to: (i) other high volume fraction reinforced composites (> 40 vol.%ceramic),[39,40] (ii) commercial particle reinforced aluminium composites,[40] and (iii) composites for

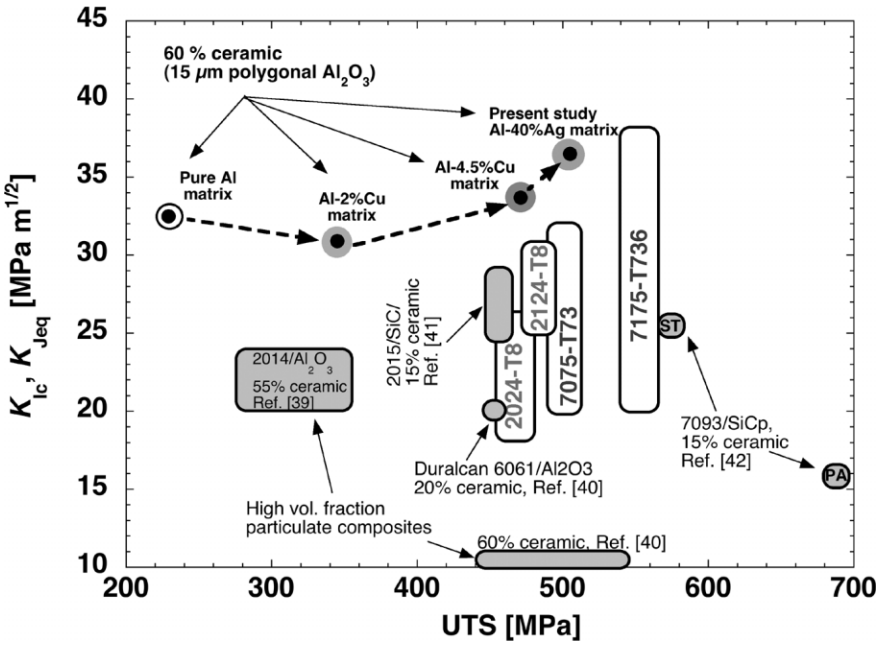

Fig. 6. Strength/toughness combination of the present Al-Ag matrix composite and comparison with (i) similar composites with matrices of pure Al and Al-Cu; (ii) high-strength unreinforced Al alloys (open boxes), [38] and (iii) selected particle reinforced aluminium composites (filled boxes).

which fairly high strength and/or toughness have been reported.[41,42] As seen, (i) with a high volume fraction of ceramic, significantly lower toughness values have been obtained elsewhere if microstructural conditions listed above are not obeyed, and (ii) in high-performance composites such as Alcoa's 7093 matrix SiC reinforced composites, strength increases are accompanied by a decrease in toughness, as in commercial aluminium alloys but contrary to what is observed here.

The much more brittle response for the as-cast Al-Ag composites confirms the crucial importance of interfacial phases in the fracture of these materials. The cohesive zone model can also suitably be applied to explain this effect, since (i) brittle intermetallics reduce the local work of fracture by creating smaller dimples,[34] and (ii) they can nucleate premature particle cracking, hence lowering the effective particle strength distribution and reducing in turn the factor by which the local work of fracture is amplified to define the global composite toughness.[2] As-cast Al-Ag composites thus behave as the Al-Cu matrix composites in the as-cast condition, for the same reason.

Conclusion: Further simultaneous increases in composite strength and toughness, above values achieved in optimal conditions with Al-Cu matrices, can be obtained with a matrix of Al-40 wt.% Ag optimally heat-treated for peak hardness and free of brittle second phases. The data from the present study thus confirm the interpretation offered earlier for toughening in this class of high-performance composites, and demonstrate the attractive strength/toughness combinations that can be achieved with appropriately designed high volume fraction ceramic particle reinforced metals.

Experimental

Materials processing and characterization: The Al-40 wt.% Ag alloy was prepared in a high vacuum laboratory furnace (Pfeiffer Balzers, model VSG 002), by induction melting. Ingots of 99.99 % pure Al (purchased from VAW Highpural GmbH, Grevenbroich, Germany) and Ag flakes (Metalor Technology SA, Neuchâtel, Switzerland), were introduced in a graphite crucible (Al:Ag wt. ratio 60:40), previously coated with zirconia to prevent attachment to the crucible wall. The vacuum chamber was initially filled with Ar prior to evacuation and subsequently induction heated. Once the alloy was molten, it was chill-cast into a graphite-coated Cu mold, to form solidified cylindrical ingots approximately 3.5 cm in diameter and 5 cm long.

The composites were fabricated by gas-pressure infiltration; details are given in Refs.[43–45] In summary, α-alumina particles (Sumicorundum™ alumina, Sumitomo, Tokyo, Japan) with an average particle size of 15 μm were packed to their natural packing density in a refractory crucible. A cast Al-Ag ingot was placed on the top of the packed powder and the crucible was inserted into a gas-infiltration apparatus. The chamber was slowly evacuated, heated to 750 °C, and infiltration was promoted by pressurizing the chamber with argon gas at 8 MPa. After infiltration was completed, directional solidification was initiated by lowering the crucible against a copper chill.

Composite microstructure was characterized using standard metallographic procedures and a field-emission SEM (Philips XL30 FEG), in the backscattered electron (BSE) detector mode, at an acceleration voltage of 10 kV. Composite density was measured by an Archimede method using a high-precision Sartorius MC210P microbalance. Samples for mechanical testing were machined by Electro-Discharge Machining (EDM). Dog-bone shaped tensile specimens were tested with a 25 kN capacity, hydraulic-driven Instron (Canton, MA, USA) universal mechanical testing machine, at a nominal strain rate of 10^{-4} s^{-1} using a clip-gauge MTS extensometer (model 632.13F-20). The Young's modulus was measured by repeated unload-reload cycling according to the procedure described by Kouzeli *et al*.[46] Fracture toughness was measured according to the ASTM standard procedure using short-bar chevron-notched fracture specimens.[47] These specimens were also machined by electro-discharge machining. The chevron-notch testing method was selected for its ability to measure the fracture toughness without the necessity to pre-crack the specimens by fatigue.[48] Tests were carried out using a Zwick (Ulm, Germany) screw-driven universal testing machine, at a displacement rate of 0.5 mm/min. The crack mouth displacement was monitored with a 632.20c-20 MTS extensometer equipped with copper arms to measure the displacement on the outer faces of the specimens. The fracture toughness was inferred from the compliance method, as described in the Standard.[47]

The heat-treatment conditions were defined so as to maximize the matrix flow stress. To this end, various heat-treatment suggested by Moore *et al*. for the Al-Ag matrix were tested,[29] and the Vickers hardness was measured using a 20 kg load, testing the composites and not the unreinforced matrix since it is well-known that ceramic particles can alter hardening characteristic of metal alloys.[49–51] It was found that (i) quenching at 350 °C (in a molten salt bath) for 30 sec and (ii) water quenching followed by peak-aging at 100 °C for 20 hs give very similar results, yielding a Vickers hardness in the range of 300 HV for the composites. This compares with values of about 260 HV for Al-4.5 wt.%Cu matrix composites in the peak-aged (T6) condition. Unreinforced matrix hardness values showed the same trend: the hardness of the Al-40 %Ag alloy (peak-aged) is 150 HV, whereas that of the Al-4.5 %Cu alloy (peak-aged) is 110 HV. Of the two heat-treatment schedules, the simpler was therefore used: after homogeneization in the single ⊖-phase field (550 °C for 20 hs), all mechanical test samples were water-quenched and subsequently aged at 100 °C for 20 hs. Additionally, tensile and fracture toughness tests were also performed on the composites in the as-cast condition (AC composites) and after solution treatment followed by quenching in water without artificial aging (T4 condition).

Received: August 26, 2005
Final version: September 30, 2005

[1] A. Miserez, A. Rossoll, A. Mortensen, *Acta Mater.* **2004**, *52*, 5331.
[2] A. Miserez, R. Müller, A. Rossoll, L. Weber, A. Mortensen, *Mater. Sci. Eng.* **2004**, *A387–389*, 822.
[3] A. Miserez, A. Rossoll, A. Mortensen, *Eng. Fract. Mech.* **2004**, *71*, 2385.
[4] A. Miserez, A. Rossoll, A. Mortensen, *Acta Mater.* **2004**, *52*, 1337.
[5] V. Tvergaard, J. W. Hutchinson, *J. Mech. Phys. Solids* **1992**, *40*, 1377.
[6] V. Tvergaard, *Comput. Mech.* **1997**, *20*, 186.
[7] D. J. Lloyd, I. Jin, in *Comprehensive Compos. Mater.* Vol. 3: *Metal Matrix Compos.* Elsevier, Amsterdam, **2000**, 555.
[8] D. J. Lloyd, in *Int. Conf. on Compos. Mater. III (ICCM-III)*, Proc. Conf., London, **1990**, Elsevier Applied Science, 359.
[9] N. Eustathopoulos, A. Mortensen, in *Fundamentals of Met. Matrix Compos.* Butterworth-Heinemann, Boston, **1993**, 3.
[10] A. Miserez, S. Stücklin, A. Rossoll, C. SanMarchi, A. Mortensen, *Mater. Sci. Technol.* **2002**, *18*, 1461.
[11] A. Mortensen, M. N. Gungor, J. A. Cornie, M. C. Flemings, *JOM* **1986**, *38*, 30.
[12] J. J. Lewandowski, C. Liu, W. H. Hunt, *Mater. Sci. Eng.* **1989**, *A107*, 241.
[13] J. J. Lewandowski, in *Comprehensive Compos. Mater. Volume 3*, Vol. 3: *Met. Matrix Compos.* Elsevier, Amsterdam, **2000**, 151.
[14] M. Manoharan, J. J. Lewandowski, *Int. J. Fract.* **1989**, *40*, 31.
[15] J. K. Park, J. P. Lucas, in *Proc. Properties and Appl. of Cast Met. Matrix Comp. Proc. Conf.* Cincinnati, OH, **1996**, The Minerals, Metals & Materials Society, 171.

[16] J. P. Lucas, J. K. Park, in *11th Int. Conf. on Compos. Mater. Proc. Conf.* Gold Cost, Queensland, Australia, **1997**, Australian Composite Structures Society, 337.
[17] W. H. Hunt, T. M. Osman, J. J. Lewandowski, *JOM* **1993**, *45*, 30.
[18] M. Manoharan, J. J. Lewandowski, *Mater. Sci. Eng.* A **1992**, *150*, 179.
[19] H. R. Shakeri, Z. R. Wang, *Metall. Mater. Trans. A* **2002**, *33*, 1699.
[20] S. Ochiai, T. Araike, K. Tokinori, K. Osamura, M. Nakatani, K. Yamatsuta, *J. Mater. Sci.* **1992**, *27*, 4667.
[21] S. Ochiai, Y. Murakami, *J. Mater. Sci.* **1979**, *14*, 831.
[22] S. Ochiai, Y. Murakami, *Metall. Trans.* **1981**, *12A*, 1155.
[23] A. G. Metcalfe, M. J. Klein, in *Interfaces in Met. Matrix Compos.* Vol. 1, Acadamic Press, New York, **1974**, 127.
[24] M. K. Shorshorov, L. M. Ustinov, A. M. Zirlin, V. I. Olefirenko, L. V. Vinogradov, *J. Mater. Sci.* **1979**, *14*, 1850.
[25] A. J. McAlister, in *Binary Alloy Phase Diagrams*, ASM international, **1990**.
[26] L. F. Mondolfo, *Aluminum Alloys: Struct. and Properties (pp. 213-224)*, Butterworths, London, **1976**.
[27] J. M. Howe, H. I. Aaronson, R. Gronsky, *Acta Metall.* **1985**, *33*, 639.
[28] K. T. Moore, J. M. Howe, *Acta Mater.* **2000**, *48*, 4083.
[29] K. T. Moore, W. C. Johnson, J. M. Howe, H. I. Aaronson, D. R. Veblen, *Acta Mater.* **2002**, *50*, 943.
[30] L. M. Barker, in *ASTM STP 855; Chevron-Notched Specimens: Testing and Stress Analysis*, Proc. Conf., Louisville, KY, **1983**, ASTM, 117.
[31] T. C. Tschanz, D. K. Matlock, G. Krauss, in *Chevron-Notch Fracture Test Experience: Met. and Non-Met.* Proc. Conf., Indianapolis, IN, **1991**, Philadelphia, PA, ASTM, 26.
[32] T. J. Grant, L. Weber, A. Mortensen, *Eng. Fract. Mech.* **2000**, *67*, 263.
[33] T. L. Anderson, *Fract. Mech.* 2nd, CRC Press, **1995**.
[34] H. P. Stüwe, *Eng. Fract. Mech.* **1980**, *13*, 231.
[35] H. P. Stüwe, in *Three-Dimensional Constitutive Relations and Ductile Fracture*, Proc. Conf., Dourdan, **1981**, N-H Publishing Company, 213.
[36] M. H. Poech, H. Fischmeister, R. Spiegler, *J. Hard Mater.* **1991**, *2*, 197.
[37] L. S. Sigl, P. A. Mataga, B. J. Dalgleish, R. M. McMeeking, A. G. Evans, *Acta Metall.* **1988**, *36*, 945.
[38] I. J. Polmear, *Light Alloys – Metall. of Light Alloys*, 3rd Edition, Arnold, London, **1995**.
[39] M. L. Seleznev, A. S. Argon, I. L. Seleznev, J. A. Cornie, R. P. Mason, Paper no. 980 700, *SAE Technical Paper Ser.* **1998**.
[40] W. H. Hunt, in *Comprehensive Compos. Mater.* Vol. 3: *Met. Matrix Compos.* Elsevier, Amsterdam, **2000**, 701.
[41] D. L. Davidson, *Metall. Trans.* **1991**, *22A*, 113.
[42] A. B. Pandey, B. S. Majumdar, D. B. Miracle, *Metall. Mater. Trans.* **2000**, *31A*, 921.
[43] V. J. Michaud, in *Fundamentals of Met. Matrix Compos.* Butterworth-Heinmann, **1993**, Ch.1.
[44] C. Garcia-Cordovilla, E. Louis, J. Narciso, *Acta Mater.* **1999**, *47*, 4461.
[45] A. Mortensen, in *Comprehensive Compos. Mater.* Vol. 3: *Met. Matrix Compos.* Elsevier, Amsterdam, **2000**, 521.
[46] M. Kouzeli, L. Weber, C. SanMarchi, A. Mortensen, *Acta Mater.* **2001**, *49*, 497.
[47] ASTM, *E 1304-89: Standard Test Method for Plane-Strain (Chevron-Notch) Fract. Toughness of Metall. Mater.* American Society for Testing and Materials, Philadelphia, **1989**, 863.
[48] *ASTM – STP 1172: Chevron-Notch Fract. Test Experience, Met. and Non-Met.*, ASTM, Philadelphia, PA, USA, **1992**.
[49] S. Suresh, K. K. Chawla, in *Fundamentals of Met. Matrix Compos.* Butterworth-Heinemann, Stoneham, Mass, **1993**, 119.
[50] T. W. Clyne, P. J. Withers, *An Introduction to Met. Matrix Compos.* Cambridge University Press, Cambridge, U.K., **1993**, 509.
[51] P. B. Prangnell, in *Comprehensive Compos. Mater.* Vol. 3: *Met. Matrix Compos.* Pergamon, Oxford UK, **2000**, 61.
[52] M. Kouzeli, L. Weber, C. SanMarchi, A. Mortensen, *Acta Mater.* **2001**, *49*, 3699.

DOI: 10.1002/adem.200500194

Carbon Nanotubes Strengthened Nanophase WC-Co Hard Alloys**

By *Guo-Long Tan*,* *Xi-Jun Wu* and *Zong-Quan Li*

WC-Co hard alloy is one of the key engineering materials, which has been widely used in mechanical industry.[1] Traditionally, tungsten powders had to be fabricated through reduction of tungsten oxide minerals by hydrogen.[2,3] Once tungsten powders were fabricated, carburization of which was necessary to produce WC-Co powders. Carburization is

[*] *G. L. Tan, Prof. X. J. Wu, Prof. Z. Q. Li*
Department of Materials Science and Engineering
Zhejiang University
Hangzhou 310027, China
E-mail: gltann@yahoo.com

[**] *The assistance of hot pressing process at Prof. Hui Yang's group, Department of Materials Science, Zhejiang University is acknowledged. The microhardness measurement at the Beijing Institute of Mechanics, Chinese Academy of Science and the financial support from Shanghai Institute of Ceramics, Chinese Academy of Science are acknowledged.*